Nuclear Instruments and Methods in Physics Research A 776 (2015) 27–33

Contents lists available at ScienceDirect

Nuclear Instruments and Methods in Physics Research A

journal homepage: www.elsevier.com/locate/nima

Numerical investigation of the radiation characteristics of a variable-period helical undulator

Kitae Lee [a,*], Jungho Mun [a], Seong Hee Park [a,b], Kyu-Ha Jang [a], Young Uk Jeong [a], Nikolay A. Vinokurov [a,c,*]

[a] Center for Quantum-Beam-based Radiation Research, Korea Atomic Energy Research Institute, Daejeon, Korea
[b] Physics Department, Chungnam Nat'l University, Daejeon, Korea
[c] Budker Institute of Nuclear Physics SB RAS, Novosibirsk, Russia

ARTICLE INFO

Article history:
Received 3 December 2013
Received in revised form
3 December 2014
Accepted 12 December 2014
Available online 22 December 2014

Keywords:
Free electron laser
Helical undulator
Spontaneous emission

ABSTRACT

A helical undulator with a variable-period capability has been developed at the Korea Atomic Energy Research Institute (KAERI) to generate high power radiation in the terahertz range. A simulation code for the spontaneous emission from an electron beam inside an undulator has been developed to characterize the performance of the undulator. In the case of the KAERI undulator, there is a non-negligible high-order harmonics in the longitudinal field distribution compared with a bifilar one.The axial velocity modulation by the high-order harmonics in the field distribution has been found to lead to small deviation of the spectrum of spontaneous emission from the KAERI undulator with respect to the bifilars one. The gain functions obtained from the spontaneous emission spectra according to the Madey theory, show similar shapes for both undulators.

1. Introduction

Free electron lasers (FELs) [1] are famous for its wavelength tuning ability, which is usually realized by changing the magnetic field strength of an undulator through varying the gap distance of the undulator magnets or current in the case of an electromagnetic undulator. As an alternative way for wavelength tuning, a helical undulator with a variable-period capability has been developed at the Korea Atomic Energy Research Institute (KAERI) [2] to generate high power radiation at around 1 THz. Since the variation of the field strength is small as the period changes, the amplification gain can be kept almost constant in changing the lasing wavelength. The combination of the variable-period helical undulator and a compact microtron accelerator can realize a table-top FEL in the terahertz range.

The performance of the newly proposed KAERI undulator has been numerically investigated. Instead of a detailed simulation on the lasing dynamics, spontaneous emission spectra from the KAERI undulator with an electron beam from the microtron accelerator are compared with a bifilar one. There is a small discrepancy in the dynamics of an electron beam, which is caused by a high-order component in the field distribution of the KAERI undulator. The small-signal gain is almost the same for both undulators. The gain functions are also compared for the case when the central frequency of both undulators are set to same by changing the undulator period of the bifilar one, which also shows very similar shapes.

2. Numerical methods

A numerical code to investigate the performance of an undulator through a spontaneous emission spectrum is developed. The code consists of two parts, one for the evaluation of electron beam dynamics and the other for the generation of a spontaneous emission spectrum. In the electron beam dynamics part, the dynamics of each electron is evaluated by the relativistic Lorentz equation under an undulator magnetic field only. Then, the dynamics of every electron is fed into the spontaneous emission part to generate angular spectral intensities at a given direction using the Lienard–Wiechert potential, then all the radiations from electrons are incoherently added to produce the total spectrum.

2.1. Electron beam dynamics

Under the assumption that the space charge effect is negligible, the dynamics of each electron under an undulator magnetic field is evaluated by the following relativistic Lorentz equations written in

* Corresponding authors.
E-mail address: klee@kaeri.re.kr (K. Lee).

http://dx.doi.org/10.1016/j.nima.2014.12.052
0168-9002/

Gaussian unit:

$$\gamma m_e c \frac{d\vec{u}}{dt} = -e\vec{u} \times \vec{B}, \tag{1}$$

where m_e and e are the electron mass and charge, respectively. c is the speed of light in vacuum. γ is the relativistic Lorentz factor, and $\vec{u} = \gamma \vec{v}$, where $\vec{v}$ is the velocity of an electron divided by c. The Boris method [3] is adopted to integrate above equation.

The initial electrons can be prepared either by listing up all the initial conditions of electrons or by sampling from a Gaussian distribution given the electron beam parameters. The Gaussian distribution for an electron beam in spatial position (x, y, z), transverse velocities normalized by the longitudinal velocity (x', y'), and energy (E) is expressed by the following formula:

$$f(x,x',y,y',z,E) = \frac{1}{(2\pi)^3 \sigma_E \sigma_z \epsilon_x \epsilon_y} \exp\left[-\frac{\gamma_x x^2 + 2\alpha_x x x' + \beta_x x'^2}{2\epsilon_x} - \frac{\gamma_y y^2 + 2\alpha_y y y' + \beta_y y'^2}{2\epsilon_y} - \frac{(E-E_o)^2}{2\sigma_E^2} - \frac{(z-z_o)^2}{2\sigma_z^2} \right], \tag{2}$$

where $\alpha_{x,y}$, $\beta_{x,y}$, and $\gamma_{x,y}$ are Twiss parameters in the x and y directions and satisfy $\gamma_{x,y} = (1+\alpha_{x,y}^2)/\beta_{x,y}$ [4]. E_o is the nominal beam energy, σ_E is the energy spread, σ_z is the longitudinal beam length, and $\epsilon_{x,y}$ are the transverse emittances. Twiss parameters and emittances are related with the transverse beam size $\sigma_{x,y}$ and the beam divergence $\theta_{x,y}$ by the following relations:

$$\gamma_{x,y} = \theta_{x,y}^2 / \epsilon_{x,y}, \tag{3}$$

$$\beta_{x,y} = \sigma_{x,y}^2 / \epsilon_{x,y}. \tag{4}$$

The beam parameter can be defined either by the Twiss parameters, or by the beam sizes and the divergences in the transverse directions.

2.2. Spontaneous emission

Once the dynamics of an electron beam is obtained, the angular spectral intensity of the spontaneous emission from each electron toward the direction $\hat{n}$ is calculated by the followings [5]:

$$\frac{d^2 I}{d\omega d\Omega} = 2\left|\vec{A}(\omega)\right|^2, \tag{5}$$

$$\vec{A}(\omega) = \frac{1}{\sqrt{2\pi}} \int_{\infty}^{\infty} \vec{A}(t) e^{-i\omega t} dt, \tag{6}$$

$$\vec{A}(t) = \sqrt{\frac{e^2}{4\pi c}} \left[\frac{\hat{n} \times \{(\hat{n} - \vec{v}) \times \dot{\vec{v}}\}}{(1 - \hat{n} \cdot \vec{v})^3} \right]_{t'}, \tag{7}$$

where $\dot{\vec{v}}$ is the time derivative of $\vec{v}$ and t' is the electron's time or retarded time, which is related to t by

$$t = t' + \frac{x - \hat{n} \cdot \vec{r}(t')}{c}, \tag{8}$$

where x is the distance from the origin to a detector under the condition of $x \gg |\vec{r}|$. All the radiations from the electrons in an electron beam are then incoherently added in the angular frequency space.

3. Results and discussions

For a comparative study, the dynamics of an electron beam in the KAERI undulator is compared with a bifilar one. The first harmonic magnetic field of the bifilar undulator is expressed in the cylindrical coordinate as follows [6]:

$$\vec{B} = 2B_u f(z) \left[\hat{e}_r I_1'(k_u r) \cos\chi - \hat{e}_\phi \frac{1}{k_u r} I_1(k_u r) \sin\chi + \hat{e}_z I_1(k_u r) \sin\chi \right], \tag{9}$$

where I_1 is the modified bessel function of order one and $\chi = \phi - k_u z$. I_1' is the derivative of the I_1 by $k_u r$. B_u is the amplitude of the undulator field and $k_u = 2\pi/\lambda_u$ with the period of the undulator λ_u. The adiabatic field at the entrance and the exit sections of the undulator is expressed by $f(z)$, which can be formulated as follows:

$$f(z) = \begin{cases} \sin^2\left(\frac{\pi}{2}\frac{z}{\Delta z_i}\right), & 0 \le z < \Delta z_i \\ 1, & \Delta z_i \le z < N_u\lambda_u - \Delta z_f \\ \sin^2\left(\frac{\pi}{2}\frac{(z - N_u\lambda_u)}{\Delta z_f}\right), & N_u\lambda_u - \Delta z_f \le z < N_u\lambda_u \\ 0, & \text{otherwise} \end{cases} \tag{10}$$

where Δz_i and Δz_f are the length of adiabatic sections at the entrance and the exit sections, respectively. N_u is the total number of periods including adiabatic sections.

At KAERI, a variable-period helical undulator has been developed [2]. As shown in Fig. 1, the basic module is composed of two iron poles and two permanent magnets embedded in a non-magnetic plate. The magnetizations of the two magnets in the module are in opposite directions $\pm z$. The base plates are arranged with a 90° rotation in series, thus four plates complete one period of a helical magnetic field distribution. Since the base plates are balanced by a repulsive force next to adjacent plates, the undulator period can be adjusted by changing the position of an end plate [2], which makes it possible to adjust the period between 2.3 cm and 2.6 cm.

For the case of $\lambda_u = 2.3$ cm, magnetic field distributions are compared between the bifilar and KAERI undulators in Fig. 2. In the case of the KAERI undulator, the field distribution was numerically obtained by the CST code [2]. The comparison of the undulators was made at the same value of the peak field B_u. One can see that there are additional high-order oscillations over a 2.3 cm oscillation in B_x of the KAERI undulator (Fig. 2(a)). It has been found that the next higher-order component to the fundamental one is the 3rd order by the Fourier transformation. The field distributions of the KAERI undulator on the axis can be described as follows:

$$B_x = A_1 \cos(k_u z) + A_3 \cos(3k_u z), \tag{11}$$

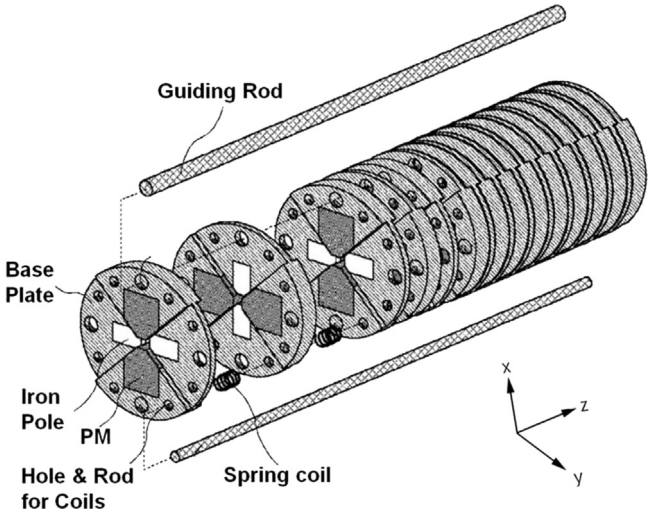

Fig. 1. Schematic of a variable-period helical undulator developed at KAERI. Each base plate is composed of two iron poles and two permanent magnets embedded in a non-magnetic plate. Each plate is arranged in series with a 90° rotation to make a helical field distribution.

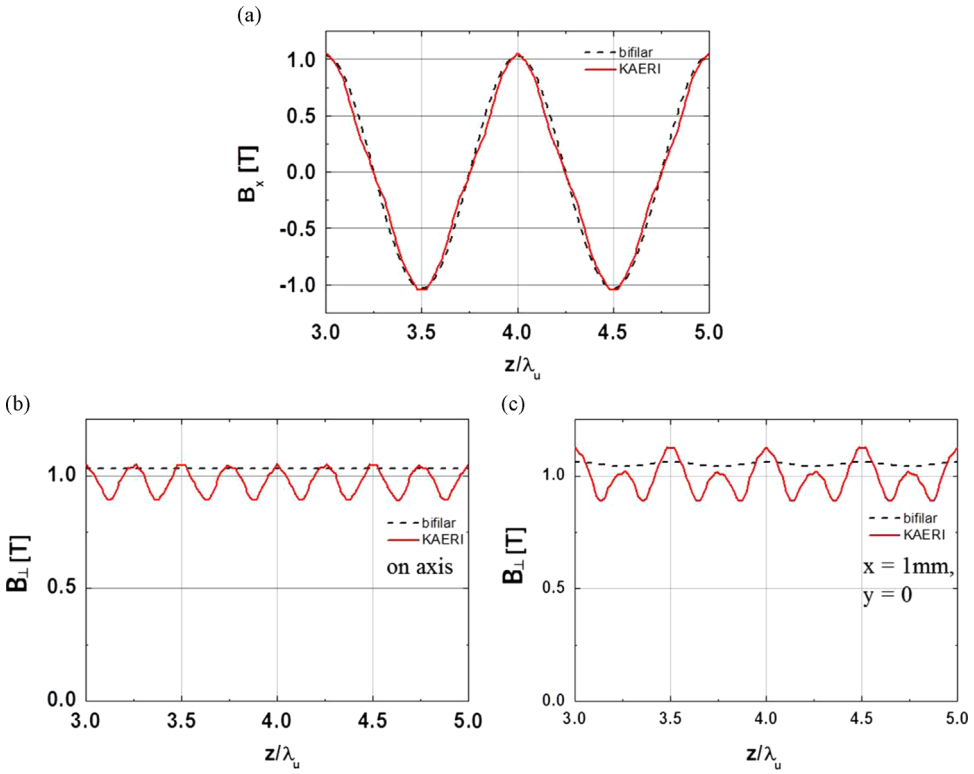

Fig. 2. Comparison of magnetic field distributions between the bifilar and KAERI undulators for $\lambda_u = 2.3$ cm: (a) B_x, (b) $B_\perp$ on axis, and (c) $B_\perp$ on $x=1$ mm and $y=0$. One can see that there is a high order harmonics of the longitudinal field distributions and its gets higher away from the axis in the case of the KAERI undulator.

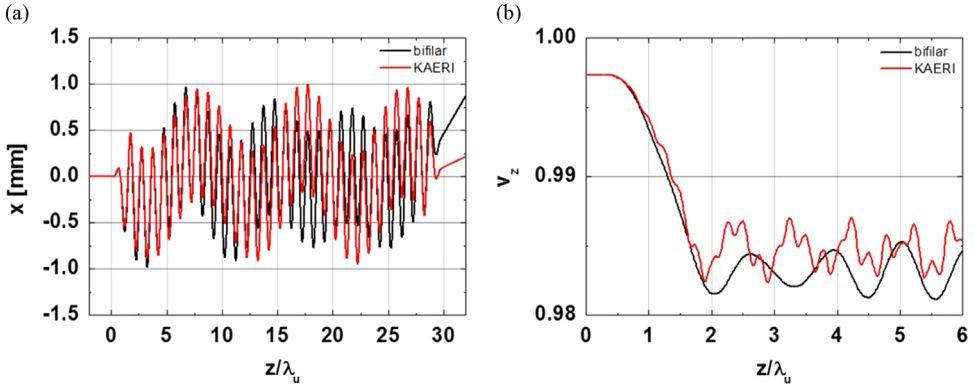

Fig. 3. Comparison of electron dynamics between the bifilar and KAERI undulators: (a) x on z and (b) v_z on z. The high order harmonics in the longitudinal field distribution in the KAERI undulator leads to a high frequency oscillation and higher axial velocity compared with the bifilar one.

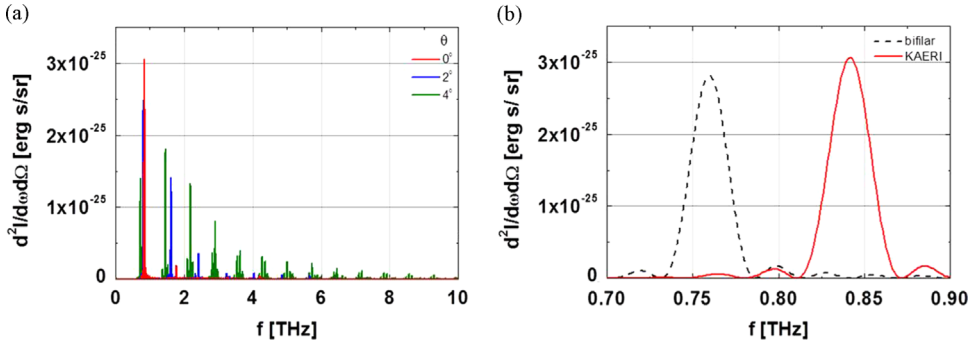

Fig. 4. Spectral intensities for the KAERI undulator on different directions ($\theta = 0^\circ$, 2°, and 4°) are plotted in (a), which shows stronger high order harmonic lines as the directions gets off the axis. The fundamental line spectra toward the axial direction for the bifilar and KAERI undulators are plotted in (b).

$$B_y = A_1 \sin(k_u z) - A_3 \sin(3k_u z), \quad (12)$$

where $A_1 \simeq 9.7$ kG, and $A_3 \simeq 0.8$ kG. This leads to the fourth order oscillation over a uniform field distribution in the transverse field strength, $B_\perp$ as shown in Fig. 2(b) and such a high-order component gets higher at off-axis (Fig. 2(c)), which makes the field strength exerted on the electron be effectively reduced by around 10% compared with the bifilar undulator. It should be mentioned that such a high-order component in the KAERI undulator makes it difficult to reduce a betatron oscillation with the adiabatic section described above, while the betatron oscillation in the bifilar undulator can be significantly reduced with increasing the adiabatic section.

For the numerical simulation, the magnetic fields are sampled at pre-specified grid points in a confined transverse dimension and several periods in the longitudinal direction. Then, in the calculation of electron dynamics, the magnetic fields at the position of an electron are obtained by the spline interpolation from the sampled data.

Table 1
The electron beam parameters used in the simulations. The negative sign in the divergence angles represents a converging beam. The corresponding Twiss parameters are also listed in the right column. The symbols listed are described in Section 2.1.

Parameter	Value	Parameter	Value
E_o	6.5 MeV		
Δ_E	0.4%		
σ_z	3 mm		
σ_x	809.3 μm	α_x	2.223
σ_y	317.2 μm	α_y	1.053
ϵ_x	1.5 mm mrad	β_x	43.66 cm
ϵ_y	0.35 mm mrad	β_y	28.75 cm
θ_x	4.5 mrad	γ_x	0.1361 cm^{-1}
θ_y	1.6 mrad	γ_y	0.07335 cm^{-1}

3.1. Single electron case

Prior to a Gaussian electron beam calculation, a single electron is investigated to characterize the KAERI undulator. Fig. 3 compares the electron motions in the two different undulators. In this calculation, an electron with an energy of 6.5 MeV enters the undulator through the axis without a transverse motion. For all of the undulators, $B_u = 10.32$ kG, $\lambda_u = 2.3$ cm, $\Delta z_i = \Delta z_f = 2\lambda_u$, and $N_u = 30$ were used. In the case of the KAERI undulator, B_u represents the maximum field strength on the axis. For both undulators, the electron is well confined near the axis owing to radial gradient of the undulator field, which also leads to a betatron oscillation as shown in Fig. 3(a). The variation of the axial velocity along the undulator is also plotted in Fig. 3(b). Reduction of the axial velocity in the adiabatic section and oscillation with period of λ_u are shown in both undulators. The axial velocity for the bifilar undulator is $v_{z,avg} = 0.9833$, while the higher axial velocity for the KAERI undulator, $v_{z,avg} = 0.9849$, comes from the lower effective field strength shown in Fig. 2. $v_{z,avg}$ is the average axial velocity in the main section of the undulator, which can be obtained by Fourier transformation of the axial velocity, thus taking zero frequency component. In the case of the KAERI undulator, a high-order oscillation is imposed on v_z over the fundamental oscillation, which is originated from the high-order component in the undulator field.

The spectral intensities of the spontaneous emission are plotted in Fig. 4, which were obtained from the previous electron dynamics. The spontaneous emission spectra from the KAERI undulator (Fig. 4(a)) shows that the high-order harmonic lines get stronger as the direction of the radiation gets off the axis,

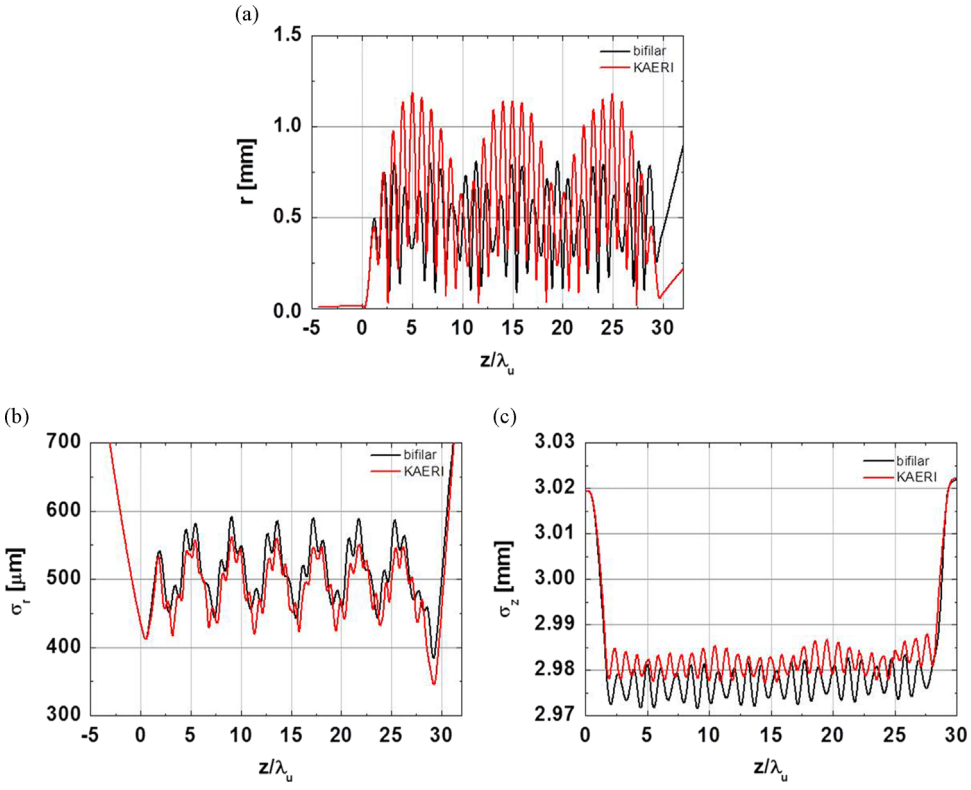

Fig. 5. For the bifilar and KAERI undulators, the radial positions of the electron beam along the undulators are plotted in (a) and the variations of the radial beam size and the beam length are plotted in (b) and (c), respectively.

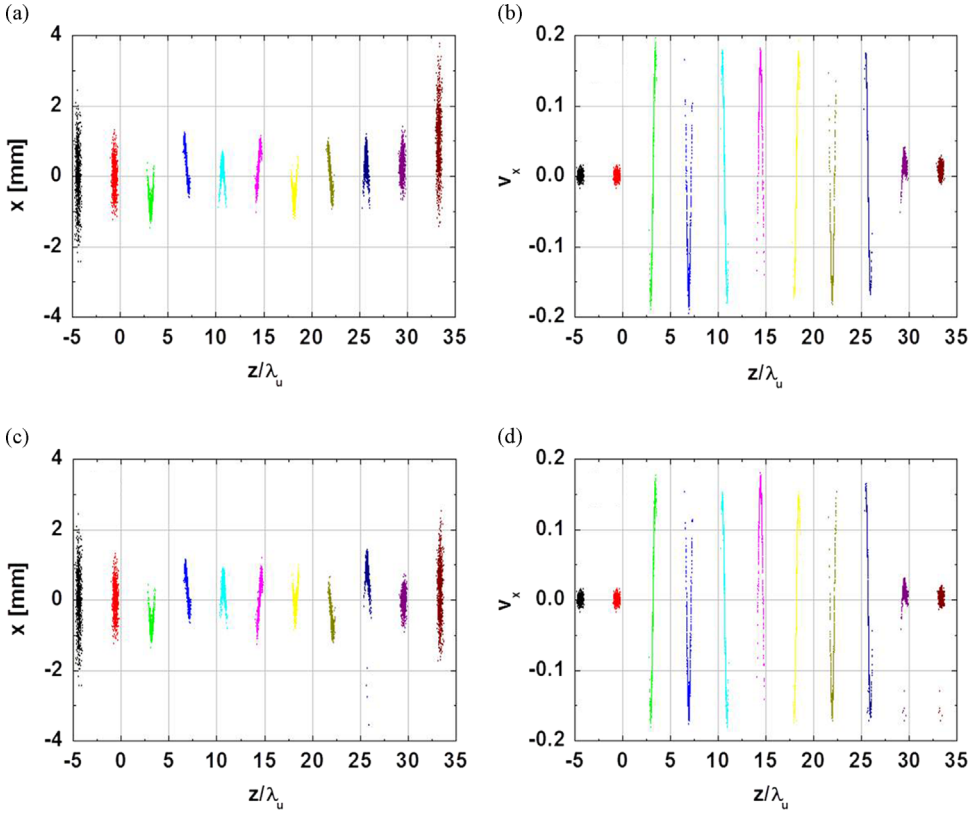

Fig. 6. Particle distributions for different times for the bifilar undulator ((a) and (b)) and for the KAERI undulator ((c) and (d)). Time interval between adjacent group is 0.3 ns and the most left ones are the initial distributions.

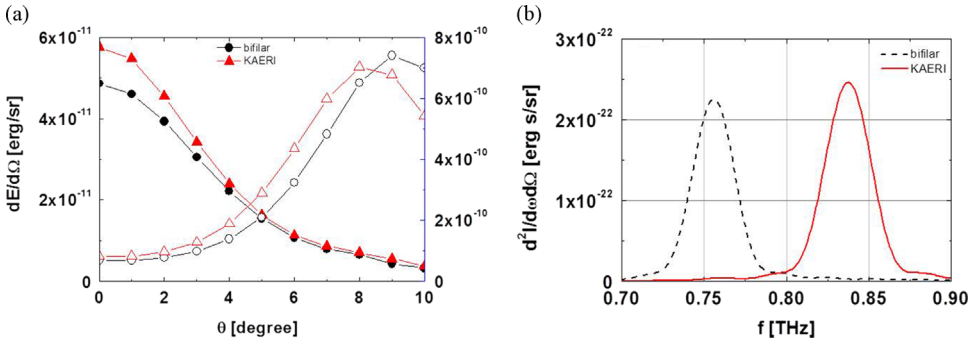

Fig. 7. Angular distributions of radiation energy are plotted for the bifilar and KAERI undulators in (a), where θ is the angle from the z axis. The filled symbols are for the fundamental line only and the empty symbols for all radiations including high order harmonics. The spectral intensities of the fundamental lines at $\theta=0^\circ$ are compared in (b).

which is a typical characteristic of the spontaneous emission from an undulator. The fundamental lines are compared in Fig. 4(b). The central frequencies are 0.76 and 0.84 THz for the bifilar and KAERI undulators, respectively. In the case of an ideal undulator, the central frequency is expressed by the following formulae:

$$f_c = \frac{1}{\lambda_u}\frac{cv_{z,avg}}{1-v_{z,avg}}. \tag{13}$$

The spectral broadenings are also well in the range of $1/N_u$, and are 24 and 27 GHz for the bifilar and KAERI undulators, respectively. These results show that even though the detailed field distribution of the KAERI undulator is different from the bifilar one, the characteristics of the spontaneous emission are quite similar except the shift of the central frequency by 10%. The last

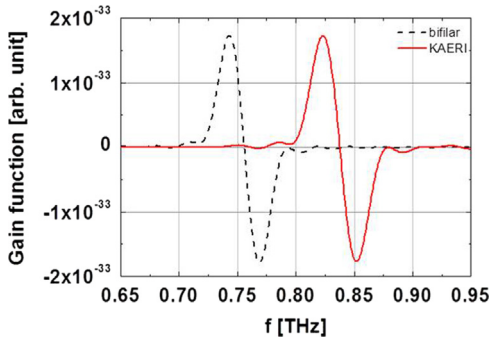

Fig. 8. The gain functions, which are obtained by derivatives of the angular spectral intensities (Fig. 6(b)) on ω are plotted for the bifilar and KAERI undulators.

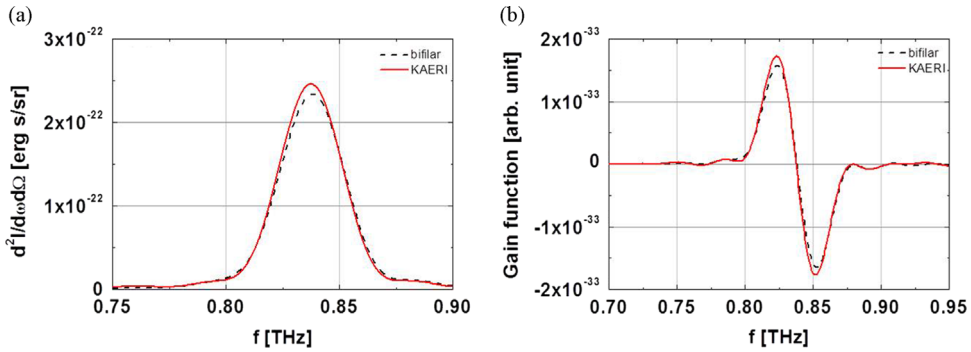

Fig. 9. For the case that the resonance frequency of the bifilar undulator is set to same with that of the KAERI one by changing the undulator period to 2.218 mm, (a) the angular spectral intensity of the spontaneous emission and (b) the gain function are compared, which shows very similar characteristics.

one is mainly caused by the lower value of the fundamental Fourier harmonics of the KAERI undulator magnetic field (at the same peak value of the fields in bifilar and KAERI undulators).

3.2. Gaussian electron beam case

For a Gaussian beam, electron beam parameters were chosen from a beam optics design. Since a cylindrical waveguide with a diameter of 4 mm is going to be installed on the axis of the KAERI undulator to enhance the beam-radiation coupling, electron-beam optics were designed to focus an electron beam at near the entrance of the undulator. The electron beam is going to be focused at $z=5$ mm with $\sigma_x = 307$ μm and $\sigma_y = 182$ μm when there is no undulator. The beam parameters of the Gaussian beam at $z = -10$ cm used in the simulations are listed in Table 1.

Fig. 5(a) shows the radial positions of the electron beam along the undulators, and its variations in sizes are also plotted in (b) and (c). Considering the radial position and radial beam size altogether, as shown in Fig. 5(a) and (b), the beam is well confined within 3 mm in diameter for both undulators. It also shows that the electron beam can be confined in a smaller region in the case of the bifilar undulator than that of the KAERI undulator by 0.3 mm in radius. For the bifilar and KAERI undulators, the radial positions of the electron beam undergo a betatron oscillation over the undulator oscillation, while the radial sizes show an oscillation with half of the betatron oscillation in period. The beam lengths also show the same oscillation with the period of the undulator as shown in Fig. 5(c) with a larger modulation but smaller variation compared with the bifilar undulator.

The particle distributions at different times on $z-x$ and $z-v_x$ are compared between the bifilar (Fig. 6(a) and (b)) and the KAERI (Fig. 6(c) and (d)) undulators, which show very similar distributions. These comparisons confirm that the dominant features of the electron beam dynamics in the KAERI undulator are quite similar with those in the bifilar one.

The total spontaneous emission from the Gaussian beam was obtained by an incoherent summation of all radiations from each electron. Fig. 7(a) shows the angular distribution of the radiation energies for fundamental lines only (filled symbols), and including all the harmonic lines (empty symbols). The fundamental lines are peaked at the axis and their angular spreads are well described by $\Delta\theta \sim 1/\gamma$, which is 4.2°. However, when the harmonic lines are included, the maximum radiation energy appears at $\theta=8$–9°. The spectral intensities of the fundamental lines at $\theta=0°$ are compared in Fig. 7(b). They show same central frequencies with the single electron case (Fig. 4(b)), while the spectral broadenings are increased to 30 and 32 GHz for the bifilar and KAERI undulators, respectively.

According to Madey's theory [7], the amplification gain of the radiation in the undulator, or the gain function can be estimated from the derivative of the spectral intensity of the spontaneous emission on the angular frequency. Fig. 8 compares the gain functions of both undulators. Except the shift of the central frequency or resonance frequency, the gain functions are very similar for the undulators considered. The peak value of the gain function for the KAERI undulator is almost the same with that of the bifilar undulator.

A simulation also has been conducted by setting the central frequency of the spontaneous emission from the bifilar undulator same with that from the KAERI undulator by reducing the undulator period of the bifilar one to 2.218 cm. As shown in Fig. 9, the spectral intensity and its gain function of the KAERI undulator are almost same with those of bifilar one, except a little higher peak value by 8%.

4. Summary and discussions

KAERI has developed a helical undulator with variable-period capability for the generation of high power radiation near 1 THz. The KAERI undulator has been found to have a high-order harmonics in the longitudinal field distribution compared with a bifilar undulator. A computational code has been developed to investigate the performance of the KAERI undulator. Instead of a detailed simulation of a lasing dynamics, the code evaluates the dynamics of an electron under an undulator field only, and a spontaneous emission spectrum from the electron beam is then calculated by an incoherent summation of individual radiations.

The dynamics of an electron beam inside the KAERI undulator shows a high-order oscillation compared with other undulators due to the high-order harmonics in the field distribution. However, the spontaneous emission spectrum, or the gain function of the KAERI undulator is very similar with those of bifilar one. When the central frequency of the bifilar undulator is set to same with that of the KAERI one, it also shows almost same gain function with a difference in the peak value by 8%. These results show that the performance of the KAERI undulator is good enough for the generation of strong radiation in the THz range as a free electron laser and an analytical estimation can still be applied for a prediction of the performance.

Acknowledgment

This work was supported by the World Class Institute (WCI) program of the National Research Foundation of Korea (NRF) funded by the Ministry of Science, ICT and Future Planning (NRF Grant number: 2011-001).

References

[1] W.B. Colson, C. Pellegrini, A. Renieri, J.M.J. Madey, Introduction to free electron laser, in: W.B. Colson, C. Pellegrini, A. Renieri (Eds.), Laser Handbook, vol. 6, Elsevier Science Pub., North-Holland, 1990.
[2] J. Mun, Y.U. Jeong, N.A. Vinokurov, K. Lee, K.-H. Jang, S.H. Park, M.Y. Jeon, S.-I. Shin, Physical Review Special Topics: Accelerators and Beams 17 (2014) 080701.
[3] C.K. Birdjall, A.B. Langdon, Plasma Physics via Computer Simulation, IOP Pub., New York, 1991 (Chapter 15).
[4] M. Conte, W.W. Mackay, An Introduction to the Physics of Particle Accelerators, World Scientific Pub., Singapore, 2008 (Chapter 5).
[5] J.D. Jackson, Classical Electrodynamics, 2nd ed., Wiley, New York, 1975 (Chapter 14).
[6] W.B. Colson, Classical free electron laser theory, in: W.B. Colson, C. Pellegrini, A. Renieri (Eds.), Laser Handbook, vol. 6, Elsevier Science Pub., North-Holland, 1990.
[7] J.M.J. Madey, Nuovo Cimento 50 (1979) 64.